Off-fault Focal Mechanisms not Representative of Interseismic Fault Loading Suggest Deep Creep on the Northern San Jacinto Fault

M. L. Cooke[1] and J. L. Beyer[1]

[1]Geosciences Department, University of Massachusetts – Amherst, USA

Corresponding author: Michele Cooke (cooke@geo.umass.edu)

Key Points:

- Crustal deformation models demonstrate the plausibility of deep creep along the northern San Jacinto fault to account for nearby enigmatic normal slip mechanisms
- Microseismicity that records off-fault deformation may record stresses that differ from interseismic loading of the primary fault surfaces
- Where faults exhibit creep at any crustal level, caution should be used in the inversion of nearby focal mechanisms for interseismic fault loading

Abstract

Within the San Bernardino basin, some focal mechanisms show normal slip that is inconsistent with the expected interseismic strike-slip loading of the region. The discrepancy may owe to deep (> 10 km depth), creep along the nearby northern San Jacinto fault. The enigmatic normal slip microseismicity occurs to the northeast of the fault and primarily below 10 km depth, consistent with off-fault deformation due to spatially non-uniform on-going slip. Consequently, if these normal focal mechanisms are included in stress inversions from the seismic catalog, the results may provide inaccurate information about fault loading. Here, we show that off-fault loading from models with deep interseismic creep on the northern San Jacinto fault match the first-order pattern of observed normal slip focal mechanisms in the basin and that this deep creep cannot be detected with GPS data due to the proximity of the San Andreas fault.

Plain Language Summary

Over the past 36 years, seismic stations have recorded the style of deformation from thousands of small earthquakes in the San Bernardino basin, California. Within this basin, many earthquakes below 10 km depth show deformation that doesn't match what we expect for this region during the current period between large damaging earthquakes along the San Jacinto and San Andreas faults. Rather than showing expected horizontal slip, many of these earthquakes show vertical movement. We use crustal deformation models to show that vertical movement can be produced in the basin if the northern portion of the San Jacinto fault creeps at depth; this portion of the fault is constantly moving rather than locked, like the San Andreas fault. Traditional GPS-based approaches to detect deep creep don't work here because the faults are too close to one another. The findings of this study demonstrate that small earthquakes that occur adjacent to and between faults can have very different style of deformation than the large ground rupturing earthquakes produced along active faults. This means that scientists should not use the information recorded by these small earthquakes in the San Bernardino basin to predict loading of the nearby San Andreas and San Jacinto faults.

1 Introduction

Earthquake rupture simulations that can inform regional seismic hazards are sensitive to estimates of current stress state along active faults (e.g., Harris et al., 2009; Ryan et al., 2015). Whereas borehole data from some localities can provide stress state information within the near surface, we rely exclusively on microseismicity data to inform the stress state throughout the seismogenic crust (e.g., Hardebeck & Hauksson, 2001; Heidbach et al., 2010). One assumption built into estimates of stress state from microseismicity is that the seismic catalog collected over the past several decades accurately represents the loading of active faults within California. This assumption is challenged by the limited duration of the seismic catalog compared to the 100-1000-year recurrence intervals along most faults within California. For example, in the earthquake catalog, the San Andreas fault (SAf) south of Cajon Pass has had fewer earthquakes than nearby faults (e.g. Yang et al., 2012). Although the San Andreas fault has the greatest potential for large earthquakes in southern California (e.g. Field et al., 2014), it is relatively under-sampled within the seismic catalog because the fault is locked between the times of large earthquakes. Furthermore, small earthquakes in the crust may record off-fault deformation rather than slip along the primary slip planes of active faults (Cheng et al., 2018). Where off fault deformation differs from loading of the primary faults, the stress state inferred from microseismicity may not accurately reflect the interseismic loading of the major active faults capable of producing ground rupturing earthquakes.

While we might expect the focal mechanisms from recorded microseismicity along the southern SAf system to reveal that dextral deformation dominates this system, Yang et al. (2013) show that some regions, such as the San Bernardino basin, produce predominantly normal-slip microseismicity (Fig. 1a). These focal mechanisms contrast the observations of long-term strike-slip along the nearby SAf (e.g., McGill et al., 2013, 2015) and San Jacinto fault (SJf) (e.g., Anderson et al., 2004; Onderdonk et al., 2015). The normal slip focal mechanisms also disagree with crustal deformation models of the region that show dextral interseismic loading of the region (e.g., Johnson, 2013; Loveless & Meade, 2011; Smith-Konter et al., 2011). Because dipping faults loaded in strike-slip will still produce strike-slip (e.g., Fattaruso et al., 2014), a non-vertical northern SJf, such as inferred along other portions of the SJf (Ross et al., 2017), could not explain the normal slip focal mechanisms. The observation of normal slip suggests that some of the recent microseismicity in the San Bernardino basin is not consistent with the expected strike-slip interseismic loading of the SAf and SJf flanking the basin.

Slip gradients along strike-slip faults, such as near the tips of earthquake ruptures, can produce off-fault stresses and subsequent aftershocks that differ from the loading of the faults (e.g., Hardebeck, 2014; Oppenheimer, 1990). Yang et al. (2012) report temporary changes in focal mechanism slip sense after large magnitude earthquakes in southern California. Cheng et al. (2018) report off-fault aftershocks that have different slip sense from the earthquakes that occur along the Anza segment of the San Jacinto fault, to the south of the study area of this paper. Some of the normal slip earthquakes within the San Bernardino basin have been associated with secondary normal faults revealed by geophysical imaging of the top of the basement (Anderson et al., 2004). Small normal faults trend sub-parallel to the SJf and bound the edges of a local graben that developed where the SJf changes strike (Fig. 1b). While strike-slip along the San Jacinto and/or San Andreas faults could promote extension of this graben and normal slip microseismicity in the San Bernardino basin, all faults in the region are presumed to be locked during the interseismic period of the seismic catalog. Furthermore, the last large slip event in the region was over 200 years ago in 1812 (e.g., Lozos, 2016), and the current seismic catalog should be free of effects from that earthquake. Three-dimensional deformation models of the region can simulate the interseismic accumulation of slip along faults below the seismogenic crust where the faults are presumed to be locked (Fig. 1c; e.g. Marshall et al., 2009) . Such models with 20 km locking depth consistent with the base of seismicity in this region (e.g., Yang et al., 2012) produce off-fault stress tensors at the 3D positions of focal mechanisms that show the preferred slip sense of off-fault deformation. Because this predicted slip sense assumes the presence of a preferentially oriented slip surface at each focal mechanism position, we add random noise to the model predictions equivalent to the -45˚ to 45˚uncertainty in focal mechanism rake (Yang et al., 2012). The model predicts overall strike-slip deformation of the region (Fig. 1d). Consequently, the observation of normal slip microseismicity in the San Bernardino basin remains enigmatic in this region of dextral interseismic loading.

We propose that some degree of unlocking of the San Jacinto fault could account for the observation of recent normal slip earthquakes in the San Bernardino basin. Spatially non-uniform creep at depth along the northern SJf may produce some degree of local extension within the basin. Consequently, the microseismicity in our multi-decadal catalog may record both interseismic dextral loading of the region as well as off-fault deformation associated with deep creep on the northern SJf. We use crustal deformation models to show the potential for slip to produce off-fault microseismicity that obfuscates our interpretation of fault loading from the seismic catalog.

2. Methods

2.1 Reliable catalog of focal mechanisms in the San Bernardino basin

We analyze the three-dimensional distribution of focal mechanisms in the San Bernardino basin to assess the spatial pattern of the enigmatic normal slip microseismcity. A catalog of relocated southern California focal mechanisms from January 1981 through September 2016 are available from the Southern California Earthquake Center database (Hauksson et al., 2012; Yang et al., 2012). We limit the analysis to focal mechanisms described by Yang et al. (2012) to have nodal plane uncertainty $< 45^{\circ}$. Figure 2a shows the 6108 focal mechanisms between Easting 455000 and 500000 meters UTM zone 11 and Northing 3740000 and 3795000 meters. In this region, the mean slip sense assessed with a 600-earthquake moving window remains around 1.2 during the time period of the seismic catalog, indicating overall normal and strike-slip focal mechanisms (black line on Fig. 2a).

Excluding earthquakes smaller than the magnitude completeness limit eliminates bias of including small earthquakes that are recorded because they occur close to seismic instruments. The completeness limit of the San Bernardino basin subset of the seismic catalog improves with time as seismic stations are added to the network. We calculate the evolving magnitude completeness limit using the maximum curvature method (Wiemer & Wyss, 2000) for a moving window of 600 earthquakes advanced in increments of 100 earthquakes. The magnitude completeness reduces around 2002 and 2011 so that we can define three epochs of magnitude completeness limits (red line on Fig. 2b). To determine a reliable focal mechanism catalog that exceed completeness, we exclude earthquakes smaller than M1.9 for epoch1 (1981 – 2001), smaller than M1.5 for epoch2 (2002-2010), and smaller than M1.1 for epoch3 (2011 – September 2016). The resulting catalog of 4304 reliable focal mechanisms shows consistent slip sense (1.2) throughout the 37-year catalog, suggesting that the catalog is not significantly impacted by transient changes, such as stress changes from nearby large earthquakes or anomalous periods of enhanced normal faulting (Fig. 2c).

2.2 Steady-state and interseismic crustal models of the region

To simulate the stresses in the San Bernardino basin that drive interseismic microseismicity, we have developed 3D Boundary Element Method stressing rate models that simulate interseismic loading between earthquakes using a two-step approach. For the first step, multiple earthquake cycles are simulated in a steady-state model where all portions of the fault surfaces slip. The second step of the approach implements a back-slip approach to simulate the interseismic loading of the faults, where the slip distribution from the steady-state model is applied to faults below the prescribed locking depth (e.g., Marshall et al., 2009).

For the first stage of interseismic model development, we produce a steady-state model of crustal deformation over many earthquake cycles. The model incorporates active fault surfaces of the region based on the SCEC Community Fault Model v. 4.0 (Nicholson et al., 2013; Plesch et al., 2007) and re-meshed for more uniform triangular element size and coincident nodes along fault intersections (Fig. 1c). While based on version 4.0 of the CFM, the fault model includes revised fault surfaces in the Eastern California Shear Zone and elsewhere that give better match to geologic slip rates (e.g., Fattaruso et al., 2014; Justin W. Herbert et al., 2014) and honors the mapped active fault traces of the USGS fault and fold database (USGS & CGS, 2006). The fault geometry used in this study follows that of the preferred model of Beyer et al. (in press) with revised resolution of the San Jacinto fault (average element length ~ 2.6 km). Within the 3D models, faults are extended to 35 km depth, where they merge with a horizontal crack. Deformation along this crack simulates distributed deformation below the seismogenic crust. Following Beyer et al. (in press), this study applies a plate tectonic movement equivalent to 47.5 mm/yr at 322.5° (e.g., DeMets et al., 2010) to the sides of the model that parallel plate velocity and a velocity gradient along the sides of the model perpendicular to plate velocity. Where faults meet the lateral edges of the model, the applied velocity has a step and corresponding slip rates are applied to the endmost patch of the fault to avoid slip rates going to zero at these artificial fault tips (Fig. 1c). The shear traction-free faults in the center of the model slip in response to tectonic loading and interaction with each other. This low shear traction simulates dynamic conditions when most of the fault slip occurs.

To simulate interseismic loading between large earthquakes, the interseismic models apply slip rates from the long-term model below a prescribed locking depth. Using this approach, these interseismic models can simulate deep creep. To avoid a sharp step between slipping and locked regions, fault elements within a 2.5 km high transitional band above the locking depth are prescribed 50% of the slip rate values of the long-term model. We explore the impact of varying locking depth from 7.5 to 20 km along the San Jacinto fault while all other faults have a 20 km locking depth. In all the models, stress tensors are sampled at points in the model corresponding to the three-dimensional locations of reliable focal mechanisms. This allows the model results to be directly compared to the observed seismicity.

3. Focal mechanism distribution supports deep creep along the northern San Jacinto fault

Three aspects of the three-dimensional distribution of interseismic microseismicity in the San Bernardino basin are consistent with some degree of deep on-going interseismic slip along the northern SJf. Firstly, the contrast of high rate of microseismicity along the SJf compared to the quiet nearby SAF (Fig. 3a). Observations of abundant microseismicity adjacent to creeping faults (e.g., Harris, 2017) support the inference that the SJf could have active creep whereas the SAf is currently locked. Secondly, projecting the focal mechanisms of the reliable catalog into a north-south profile reveals that most of the normal slip focal mechanisms of the San Bernardino basin occur below ~7.5 km depth (Fig. 3b). If the on-going SJf slip is contributing to the off-fault normal slip microseismicity, then the fault below this depth may be creeping. Along the Anza section of the San Jacinto fault, south of this study area, normal slip microseismicity also occurs near the SJf at depths of 10-13 km (Cheng et al., 2018). The discrepancy between locking depth of the Anza section of the SJf inferred from geodesy (11±3 km; Fialko, 2006)and the base of seismicity in this region (17±3 km) led to the inference of local creep below 10 km (Wdowinski, 2009), which is consistent with the depths of off-fault normal microseismicity along this section of the SJf (Cheng et al., 2018).

The third aspect of the focal mechanism distribution that supports deep on-going interseismic slip is that the normal slip focal mechanisms are primarily located northeast, and not southwest, of the SJf (Fig. 3a). Regional extension should produce normal slip microseismicity on both sides of interseismic locked faults. However, this pattern is consistent with the results of steady-state crustal deformation models of the region that simulate deformation over multiple earthquake cycles (Resor et al., 2018; Fig. 4b). This model shows a southward increasing dextral slip rate along the northern San Jacinto fault that produces a region of positive dilation (increased mean normal tension) within the San Bernardino basin. This long-term dilation can promote normal slip microseismicity at distances far from the fault by unclamping potential slip surfaces relative to those outside of the basin. The location of off-fault dilation correlates to the location of slip rate gradient along the SJf (Fig. 4b). Consequently, deep dilation consistent with the occurrence of normal slip microseismicity below ~7.5 km in the San Bernardino basin may be associated with on-going slip along the SJf below ~7.5 km. Deep on-going slip on the San Andreas fault could also produce dilation in the San Bernardino basin but the lack of microseismicity along the SAf suggests that this fault is locked. Taken together, the three-dimensional distribution of focal mechanisms within the San Bernardino basin is consistent with southward increasing creep rate along the northern SJf at depth.

4. Simulating deep creep on the northern San Jacinto fault

To investigate the impact of deep interseismic creep on the northern San Jacinto fault, we investigate the sensitivity of focal mechanism slip sense within the San Bernardino basin to locking depth along the northern SJf (San Bernardino and San Jacinto Valley segments). The interseismic models apply 20 km locking depth on all other faults, consistent with the general base of seismicity of the region (e.g. Yang et al., 2012; Fig. 3b). The overall slip sense of microseismicity within the San Bernardino basin (grey region in Fig. 5a) is best matched by interseismic models with locking depth < 12.5 km along the northern SJf (Fig. 5b). Results for locking depths of 7.5 and 10 km show similar fit within 1σ. The interseismic model with 10 km locking depth produces normal slip that is spatially consistent with the observed enigmatic normal slip focal mechanisms within the San Bernardino basin (Fig. 5a). The normal slip in the interseismic model occurs to the northeast of the San Jacinto fault near the gradient in dextral slip rate along the fault.

While creep below 10-13 km has been inferred along the southern San Jacinto fault from geodetic evidence of shallow locking depths (Fialko, 2006; Smith-Konter et al., 2011; Wdowinski, 2009), geodetic inversions for the northern San Jacinto fault suggest a deep (~20 km) locking depth (Smith-Konter et al., 2011). Because the San Jacinto and San Andreas faults approach within 10 km of each other at the San Bernardino basin, the inversions of geodetic data for locking depth in this region may not distinguish the locking depths of the SJf and SAf. To explore this, we compare the interseismic velocities at GPS sties from two models: one that has 20 km locking depth on all faults and another that has 10 km locking depth on the northern SJf and 20 km on all other faults. The station velocities from the two models cannot be distinguished from the observed GPS station velocities determined by Herbert at al. (2014) (Fig. 5c). Consequently, geodetic data cannot eliminate deep creep on the northern San Jacinto fault as a potential mechanism for the off-fault normal slip microseismicity within the San Bernardino basin.

5. Discussion

Both the observed focal mechanisms and the model predicted slip show both normal and strike-slip microseismicity in the San Bernardino basin. Some differences in the predicted interseismic slip sense at locations of microseismicity and observed slip sense reveal aspects of the model that may not adequately capture the 3D complexity of active deformation along the San Jacinto fault. Within the model, normal slip microseismicity occurs within a narrow band adjacent to the SJf with strike- and reverse slip outside of this band where the catalog records a combination of normal and strike-slip focal mechanisms. The model may over-predict the proportion of normal focal mechanisms for several potential reasons. Firstly, the model calculates the slip sense on the most preferentially oriented slip plane off of the fault but, if instead, the microseismicity occurs on preexisting structures, the observed slip sense may differ from the model prediction. Similarly, the model does not consider interaction between earthquakes such as local normal microseismicity after small strike-slip earthquakes (Cheng et al., 2018). Another consideration is that the model may over-predict normal slip because the model incorporates complete unlocking of the SJf below the locking depth whereas partial unlocking may provide an off-fault stress state between that of dilation and interseismic strike-slip loading of the region.

Within the model, faults that may have damage zones and complex secondary structures are modeled as single slip surfaces discretized into elements with constant slip. The nature of fault surface discretization within the model leads to artificially linear and abrupt transitions from slipping to transitional (1/2 long term slip rate) to locked portions of the fault. These abrupt transitions may produce a more localized pattern of normal slip microseismicity than observed. Furthermore, the model does not consider host rock heterogeneities and deformation along secondary faults (e.g. Anderson et al., 2004) that could act to promote interseismic normal slip microseismicity over a wider region. For example, deep creep along strands parallel to the modeled San Jacinto fault would broaden the predicted zone of off-fault normal faulting. Our analysis does not distinguish between localized creep on a single plane and a narrow zone of distributed creep, and either of these scenarios may be occurring at depth along the SJf.

A rich aftershock catalog from the recent Borrego Springs 2016 earthquake shows evidence for a distributed zone of on-going deformation along southern San Jacinto fault where it splits into three sub-parallel strands (Ross et al., 2017). A similar investigation for the northern San Jacinto fault may yield further insight into the detailed structure of the fault. For example, such a study might confirm secondary structures that were interpreted from early seismic catalogs by Nicholson et al. (1986).

Deep creep along the northern San Jacinto fault may impact seismic hazard estimates on this fault. Both the accommodation of slip along the fault and the accommodation of off-fault deformation within the adjacent crust via microseismicity and aseismic pervasive deformation mechanisms may reduce the interseismic loading on the deeper portion of the northern SJf, thereby reducing seismic hazard. We might also expect moderate or large earthquakes to nucleate at the transition between creeping and locked portions (Harris, 2017). Shallow sections of the northern SJf may have increased loading due to deep creep and greater potential for large earthquakes.

The correlation between the slip sense of focal mechanisms in the San Bernardino basin and patterns of off-fault stressing rate from interseismic models with ~10 km locking depth on the San Jacinto fault suggests that the interseismic microseismicity of the basin records a component of permanent distributed off-fault deformation in the basin. This result is consistent with a recent study of normal slip focal mechanisms along the Anza section of the SJf (Cheng et al., 2018). If the focal mechanisms of the basin were inverted to estimate interseismic stresses on the SJf and SAf, they would predict normal loading contrary to the long-term slip record of these faults. Using microseismicity that records this off-fault deformation may produce erroneous estimates of interseismic fault loading. Within the San Bernardino basin, the errors of focal mechanism inversions for fault stressing rate are compounded by the under-sampling of strike-slip earthquakes along the relatively quiet SAf. This study suggests that where faults creep, spatially non-uniform creep rates may produce heterogeneous off-fault deformation. Geodesy around the juncture of the creeping section of the San Andreas fault with the locked Carrizo section show off-fault dilation due to similar spatial gradient in creep rate as proposed here (Titus et al., 2011). Where faults exhibit creep at any crustal level, caution should be used when incorporating off-fault focal mechanisms to infer interseismic fault loading.

Acknowledgments, Samples, and Data

This research was supported by the Southern California Earthquake Center (Contribution No. 8079). SCEC is funded by NSF Cooperative Agreement EAR-1033462 & USGS Cooperative Agreement G12AC20038. Reviews by Ruth Harris, Zachary Ross and editor Gavin Hayes greatly improved this manuscript. The authors thank Scott Marshall for sharing his Poly3D executable code and many insightful discussions. Model results of slip sense sampled at locations of microseismicity for the interseismic models with various locking depth are available on figshare (Cooke, 2018).

References

Anderson, M., Matti, J., & Jachens, R. (2004). Structural model of the San Bernardino basin, California, from analysis of gravity, aeromagnetic, and seismicity data. *Journal of Geophysical Research: Solid Earth*, *109*(4). https://doi.org/10.1029/2003JB002544

Beyer, J. L., Cooke, M. L., & Marshall, S. T. (2018). Sensitivity of deformation to activity along the Mill Creek and Mission Creek strands of the San Andreas fault. *Geosphere Special Issue on Seismotectonics of the San Gorgonio Pass Region.*

Cheng, Y., Ross, Z. E., & Ben-Zion, Y. (2018). Diverse Volumetric Faulting Patterns in the San Jacinto Fault Zone. *Journal of Geophysical Research: Solid Earth*, *123*(6), 5068–5081. https://doi.org/10.1029/2017JB015408

Cooke, M. (2018). *Modeled slip style at locations of microseismicity within the San Bernardino basin, CA*. https://doi.org/10.6084/m9.figshare.6361022.v2

Craig, N., Leonardo, S., Patrick, W., & R., S. L. (1986). Seismic evidence for conjugate slip and block rotation within the San Andreas Fault System, southern California. *Tectonics*, *5*(4), 629–648. https://doi.org/10.1029/TC005i004p00629

DeMets, C., Gordon, R. G., & Argus, D. F. (2010). Geologically current plate motions. *Geophysical Journal International*, *181*(1), 1–80. https://doi.org/10.1111/j.1365-246X.2009.04491.x

Fattaruso, L. A., Cooke, M. L., & Dorsey, R. J. (2014). Sensitivity of uplift patterns to dip of the San Andreas fault in the Coachella Valley, California. *Geosphere*, *10*(6). https://doi.org/10.1130/GES01050.1

Fialko, Y. (2006). Interseismic strain accumulation and the earthquake potential on the southern San Andreas fault system. *Nature*, *441*(7096), 968–971. https://doi.org/10.1038/nature04797

Hardebeck, J. L. (2014). The impact of static stress change, dynamic stress change, and the background stress on aftershock focal mechanisms. *Journal of Geophysical Research: Solid Earth*, *119*(11), 8239–8266.

Hardebeck, J. L., & Hauksson, E. (2001). Crustal stress field in southern California and its implications for fault mechanics. *Journal of Geophysical Research: Solid Earth*, *106*(B10), 21859–21882. https://doi.org/10.1029/2001JB000292

Harris, R. A. (2017). Large earthquakes and creeping faults. *Reviews of Geophysics*, *55*(1), 169–198. https://doi.org/10.1002/2016RG000539

Harris, R. A., Barall, M., Archuleta, R., E. Dunham, E., Aagaard, B., Ampuero, J. P., et al. (2009). The SCEC/USGS Dynamic Earthquake Rupture Code Verification Exercise. *Seismological Research Letters*, *80*(1), 119–126. Retrieved from http://dx.doi.org/10.1785/gssrl.80.1.119

Hauksson, E., Yang, W., & Shearer, P. M. (2012). Waveform relocated earthquake catalog for Southern California (1981 to June 2011). *Bulletin of the Seismological Society of America*, *102*(5), 2239–2244. https://doi.org/10.1785/0120120010

Heidbach, O., Tingay, M., Barth, A., Reinecker, J., Kurfeß, D., & Müller, B. (2010). Global crustal stress pattern based on the World Stress Map database release 2008. *Tectonophysics*, *482*(1), 3–15. https://doi.org/https://doi.org/10.1016/j.tecto.2009.07.023

Herbert, J. W., Cooke, M. L., Oskin, M., & Difo, O. (2014). How much can off-fault deformation contribute to the slip rate discrepancy within the eastern California shear zone? *Geology*, *42*(1), 71–75. https://doi.org/10.1130/G34738.1

Herbert, J. W., Cooke, M. L., & Marshall, S. T. (2014). Influence of fault connectivity on slip rates in southern California: Potential impact on discrepancies between geodetic derived and geologic slip rates. *Journal of Geophysical Research: Solid Earth*, *119*(3). https://doi.org/10.1002/2013JB010472

Johnson, K. M. (2013). Slip rates and off-fault deformation in Southern California inferred from GPS data and models. *Journal of Geophysical Research: Solid Earth*, *118*(10), 5643–5664. https://doi.org/10.1002/jgrb.50365

Loveless, J. P., & Meade, B. J. (2011). Stress modulation on the San Andreas fault by interseismic fault: System interactions. *Geology*, *39*(11), 1035–1038. https://doi.org/10.1130/G32215.1

Lozos, J. C. (2016). A case for historic joint rupture of the San Andreas and San Jacinto faults. *Science Advances*, *2*(3), 1–8. https://doi.org/10.1126/sciadv.1500621

Marshall, S. T., Cooke, M. L., & Owen, S. E. (2009). Interseismic deformation associated with three-dimensional faults in the greater Los Angeles region, California. *Journal of Geophysical Research: Solid Earth*, *114*(12). https://doi.org/10.1029/2009JB006439

McGill, S. F., Owen, L. A., Weldon, R. J., & Kendrick, K. J. (2013). Latest pleistocene and holocene slip rate for the San Bernardino Strand of the San Andreas Fault, Plunge Creek, Southern California: Implications for strain partitioning within the Southern San Andreas Fault system for the last ~35 k.y. *Bulletin of the Geological Society of America*, *125*(1–2), 48–72. https://doi.org/10.1130/B30647.1

McGill, S. F., Spinler, J. C., McGill, J. D., Bennett, R. A., Floyd, M. A., Fryxell, J. E., & Funning, G. J. (2015). Kinematic modeling of fault slip rates using new geodetic velocities from a transect across the Pacific-North America plate boundary through the San Bernardino Mountains, California. *Journal of Geophysical Research: Solid Earth*, *120*(4), 2772–2793. https://doi.org/10.1002/2014JB011459

Nicholson, C., Plesch, A., Sorlien, C., Shaw, J., & Hauksson, E. (2013). Updating the 3D fault set for the Community Fault Model (CFM-v4) and revising its associated fault database. In *Southern California Earthquake Center annual meeting*.

Onderdonk, N. W., McGill, S. F., & Rockwell, T. K. (2015). Short-term variations in slip rate and size of prehistoric earthquakes during the past 2000 years on the northern San Jacinto fault zone, a major plate-boundary structure in southern California. *Lithosphere*, *7*(3), 211–234. https://doi.org/10.1130/L393.1

Oppenheimer, D. H. (1990). Aftershock slip behavior of the 1989 Loma Prieta, California earthquake. *Geophysical Research Letters*, *17*(8), 1199–1202.

Plesch, A., Shaw, J. H., Benson, C., Bryant, W. A., Carena, S., Cooke, M., et al. (2007). Community Fault Model (CFM) for southern California. *Bulletin of the Seismological*

Society of America, *97*(6). https://doi.org/10.1785/0120050211

Resor, P. G., Cooke, M. L., Marshall, S. T., & Madden, E. H. (2018). Influence of Fault Geometry on the Spatial Distribution of Long-Term Slip with Implications for Determining Representative Fault-Slip Rates. *Bulletin of the Seismological Society of America*, *XX*(Xx). https://doi.org/10.1785/0120170332

Ross, Z. E., Hauksson, E., & Ben-Zion, Y. (2017). Abundant off-fault seismicity and orthogonal structures in the San Jacinto fault zone. *Science Advances*, *3*(3). https://doi.org/10.1126/sciadv.1601946

Ryan, K. J., Geist, E. L., Barall, M., & Oglesby, D. D. (2015). Dynamic models of an earthquake and tsunami offshore Ventura, California. *Geophysical Research Letters*, *42*(16), 6599–6606. https://doi.org/10.1002/2015GL064507

Simpson, R. W. (1997). Quantifying Anderson's fault types. *Journal of Geophysical Research: Solid Earth*, *102*(B8), 17909–17919. https://doi.org/10.1029/97JB01274

Smith-Konter, B. R., Sandwell, D. T., & Shearer, P. (2011). Locking depths estimated from geodesy and seismology along the San Andreas Fault System: Implications for seismic moment release. *Journal of Geophysical Research: Solid Earth*, *116*(6), 1–12. https://doi.org/10.1029/2010JB008117

Survey, U. S. G., & Survey, C. G. (2006). Quaternary fault and fold database for the United States. Retrieved July 20, 2001, from http//earthquake.usgs.gov/hazards/qfaults/

Titus, S. J., Dyson, M., DeMets, C., Tikoff, B., Rolandone, F., & Bürgmann, R. (2011). Geologic versus geodetic deformation adjacent to the San Andreas fault, central California. *Bulletin of the Geological Society of America*, *123*(5), 794–820. https://doi.org/10.1130/B30150.1

Wdowinski, S. (2009). Deep creep as a cause for the excess seismicity along the San Jacinto fault. *Nature Geoscience*, *2*(12), 882–885. https://doi.org/10.1038/ngeo684

Wiemer, S., & Wyss, M. (2000). Minimum magnitude of completeness in earthquake catalogs: Examples from Alaska, the Western United States, and Japan. *Bulletin of the Seismological Society of America*, *90*(4), 859–869. https://doi.org/10.1785/0119990114

Yang, W., & Hauksson, E. (2013). The tectonic crustal stress field and style of faulting along the Pacific North America plate boundary in southern California. *Geophysical Journal International*, *194*(1), 100–117. https://doi.org/10.1093/gji/ggt113

Yang, W., Hauksson, E., & Shearer, P. M. (2012). Computing a large refined catalog of focal mechanisms for southern California (1981-2010): Temporal stability of the style of faulting. *Bulletin of the Seismological Society of America*, *102*(3), 1179–1194. https://doi.org/10.1785/0120110311

Figure Captions

Figure 1. a) Focal mechanisms with nodal plane uncertainty 10˚-45˚ from 1981 through September of 2016 in the relocated catalog of (Yang et al., 2012 and subsequent updates

available from SCEC) with surface traces of faults active within the last 15 ka (USGS & CGS, 2006). Colors show slip sense as rake scaled to the 0-3 slip sense range of Aϕ (Simpson, 1997). b). Basement depth inverted from gravity data shows secondary normal faults that flank the San Jacinto fault (taken from Anderson et al., 2004). The normal slip focal mechanisms extend beyond the interpreted graben. c) Model of 63 active faults in the region used to build the steady state and interseismic models of crustal deformation. The lateral edges of the horizontal crack are loaded with plate velocities to simulate the regional tectonic loading (taken from Beyer et al., in press). d) Slip sense predicted by interseismic crustal deformation model of c at locations of the earthquakes recorded in the catalog. Traces of modeled faults shown in black. Insets of a) and d) show histograms of slip sense. The normal slip focal mechanisms within the San Bernardino basin are not expected from interseismic loading of completely locked San Andreas and San Jacinto faults.

Figure 2. a) Focal mechanisms within the region of Figure 1. The average slip sense for a moving window of 600 earthquakes shown with black line. Warm colors are normal, cool colors are reverse, and green are strike-slip earthquakes b) Magnitude completeness limit for a moving window of 600 earthquakes advanced in 100 earthquake increments shown in blue. The stepped red line shows the three estimated stages of magnitude completeness during the record. C) The 4304 focal mechanisms that exceed the three-phased magnitude completeness limit have mean slip sense of 1.2 ± 0.04, indicating limited variation in slip sense during the record. These earthquakes range in magnitude from 1 to 4.8 and depths from 1.2-20 km. (d-e) The log of frequency demonstrates the completeness of the catalog for each epoch: 1981 through 2001 (d), 2002 through 2010 (e) and after 2011 (f). The completeness limit (red dashed line) decreases in each successive epoch.

Figure 3. a) Map view of reliable focal mechanisms that pass the completeness test, colored by slip sense. Normal slip focal mechanisms occur within the San Bernardino basin, between the San Andreas and San Jacinto faults. Dashed fault traces are the graben bounding normal faults imaged by Anderson (2004) in Fig. 1c. b) Focal mechanisms of the San Bernardino basin (grey region of a) projected into the A-A' profile perpendicular to the San Jacinto fault. Slip sense color same as in a). The normal slip focal mechanisms within the San Bernardino basin occur predominantly below 7.5 km depth.

Figure 4. Green arrows show the velocities from the steady state model that simulates many earthquake cycles. The divergence of this velocity field reveals regions of overall contraction (negative dilation blue) and extension (positive dilation red) due to slip distribution along the faults. Inset cartoon shows the set-up of the steady-state model.

Figure 5: a) Slip sense at locations of microseismicity from the interseismic model with locking depth of 10 km on the San Jacinto fault to simulate deep creep. The locking depth on all other faults is 20 km. Color indicates slip sense with random -45˚ to 45˚ noise added to the model results (distribution in top inset). Inset cartoon shows the set-up of the interseismic model. Normal loading occurs at focal mechanism sites within the San Bernardino basin. GPS stations shown with labeled triangles. b) Mean interseismic loading within light grey region of A shown with 1σ vertical bars. Models with SJf locking depth < 12.5 km better match the mean slip sense of focal mechanisms in the San Bernardino Basin. c) Transect along A-A' (shown in A) of GPS

station velocity parallel to the San Jacinto fault (J.W. Herbert et al., 2014), and velocity predictions from the interseismic model with a shallow locking depth on the SJf (pink star, same as results shown in A) and interseismic model with a 20 km locking depth on all faults (blue circle). The surface velocities cannot resolve deep slip on the SJf because of its proximity to the SAf.

figure 1.

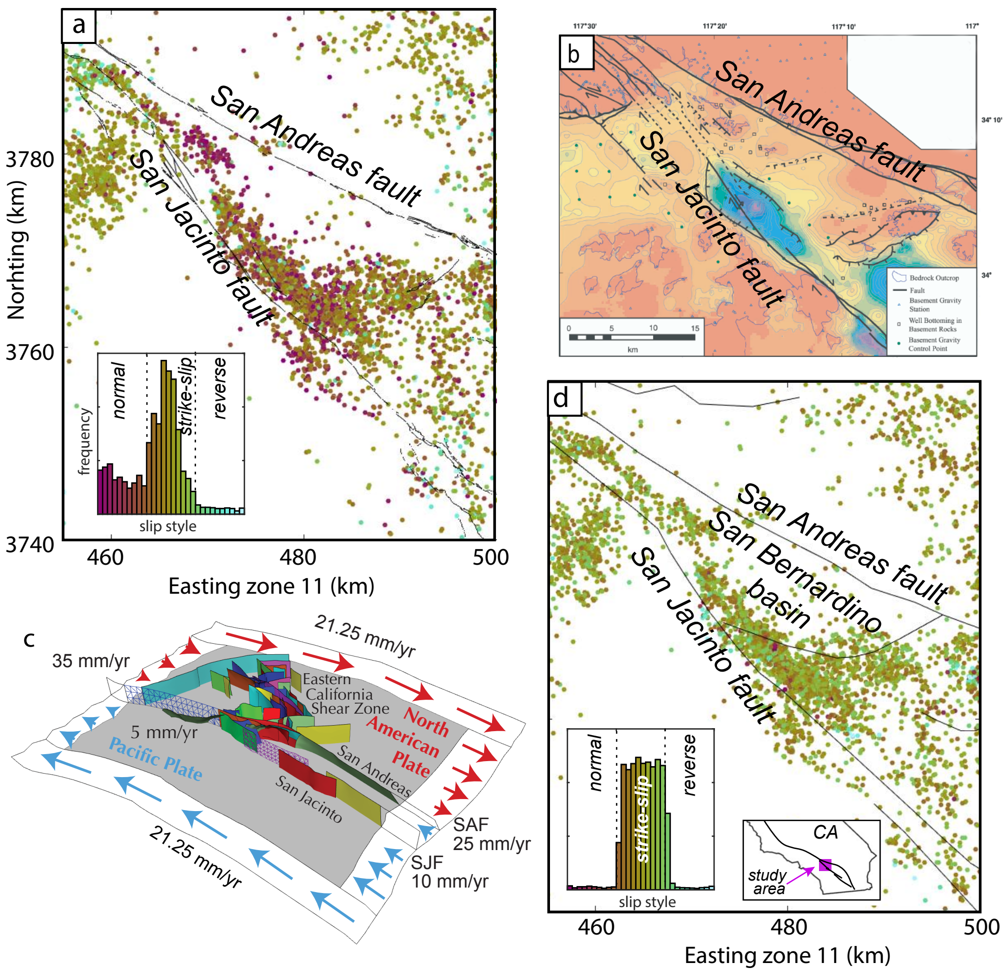
a
San Andreas fault
San Jacinto fault
Norhting (km)
3780
3760
3740
460
480
500
Easting zone 11 (km)
normal
strike-slip
reverse
frequency
slip style
b
117°30'
117°20'
117°10'
117°
34° 10'
34°
San Andreas fault
San Jacinto fault
Bedrock Outcrop
Fault
Basement Gravity Station
Well Bottoming in Basement Rocks
Basement Gravity Control Point
0
5
10
15
km
c
21.25 mm/yr
35 mm/yr
Eastern California Shear Zone
5 mm/yr
North American Plate
Pacific Plate
San Andreas
San Jacinto
SAF 25 mm/yr
SJF 10 mm/yr
21.25 mm/yr
d
San Andreas fault
San Bernardino basin
San Jacinto fault
normal
strike-slip
reverse
slip style
CA
study area
460
480
500
Easting zone 11 (km)

figure 2.

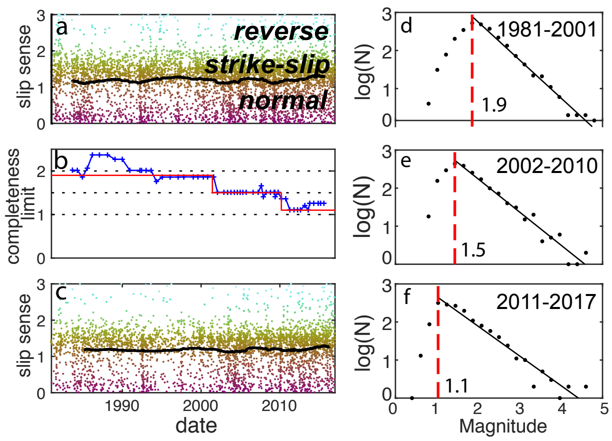
a
reverse
strike-slip
normal
slip sense
b
completeness limit
c
slip sense
date
d
1981-2001
1.9
e
2002-2010
1.5
f
2011-2017
1.1
log(N)
Magnitude

figure 3.

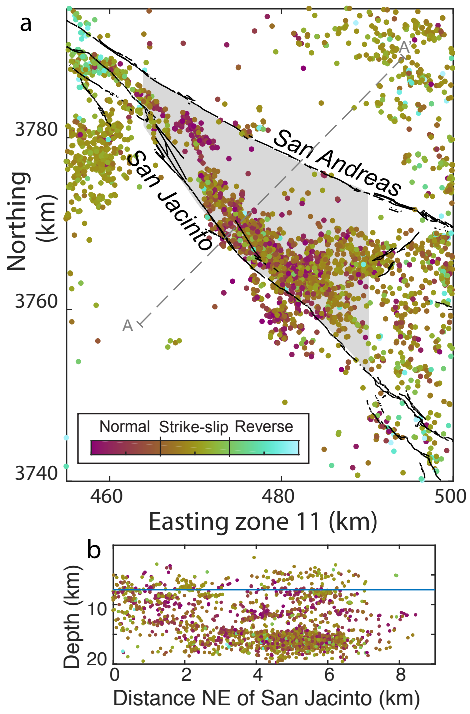

a
San Andreas
San Jacinto
A
A'
Normal
Strike-slip
Reverse
3780
3760
3740
Northing (km)
460
480
500
Easting zone 11 (km)
b
Depth (km)
10
20
0
2
4
6
8
Distance NE of San Jacinto (km)

figure 4.

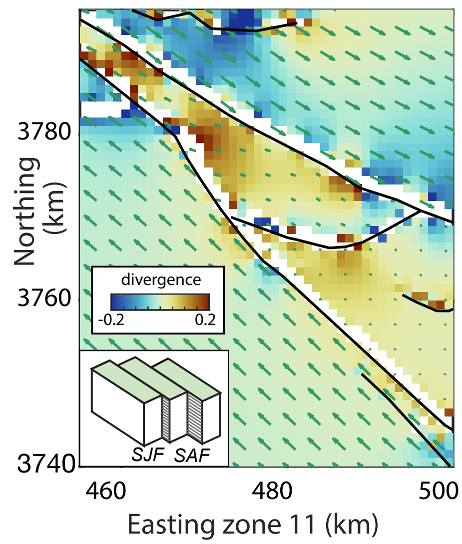

3780
3760
3740
Northing (km)
460
480
500
Easting zone 11 (km)
divergence
-0.2
0.2
SJF
SAF

figure 5.

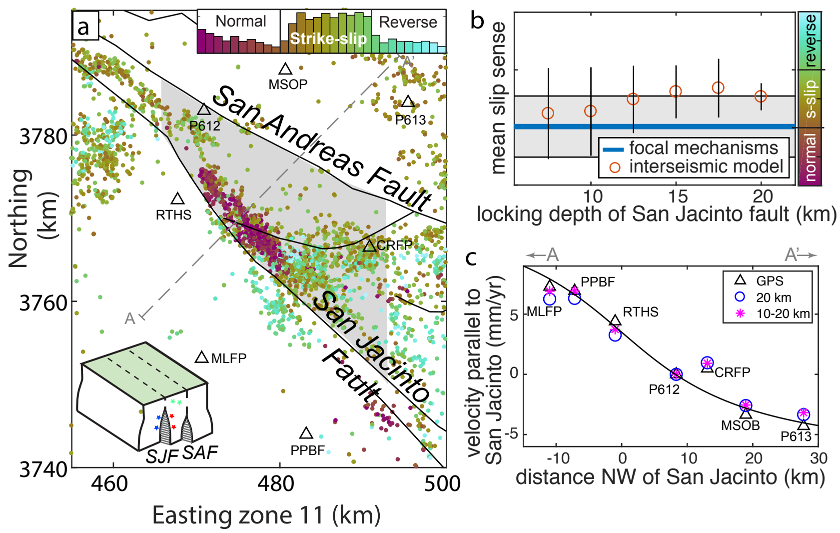

a
Normal
Strike-slip
Reverse
MSOP
P612
P613
San Andreas Fault
RTHS
CRFP
San Jacinto Fault
A
A'
MLFP
PPBF
SJF
SAF
Northing (km)
3740
3760
3780
460
480
500
Easting zone 11 (km)
b
mean slip sense
reverse
s-slip
normal
focal mechanisms
interseismic model
10
15
20
locking depth of San Jacinto fault (km)
c
velocity parallel to San Jacinto (mm/yr)
GPS
20 km
10-20 km
MLFP
PPBF
RTHS
P612
CRFP
MSOB
P613
-10
0
10
20
30
5
0
-5
distance NW of San Jacinto (km)